Scientific Research Publishing

Open Journal of Geology, 2026, 16(4), 171-196
https://www.scirp.org/journal/ojg
ISSN Online: 2161-7589
ISSN Print: 2161-7570

Stability Analysis of Underpinning Elevated Bridge Piles in Deep Foundation Pits

Fengjiang Luo[1], Hui Lu[2*], Haijun Zhou[3]

[1]China Railway 24th Bureau Group Co., Ltd., Shanghai, China
[2]Research Center of Urban Underground Space, Nanjing Tech University, Nanjing, China
[3]China Jiangsu Sci-Tech Innovation Industry Development Co., Ltd., Nanjing, China
Email: *3110375587@qq.com

How to cite this paper: Luo, F.J., Lu, H. and Zhou, H.J. (2026) Stability Analysis of Underpinning Elevated Bridge Piles in Deep Foundation Pits. *Open Journal of Geology*, **16**, 171-196.
https://doi.org/10.4236/ojg.2026.164010

Received: January 22, 2026
Accepted: April 10, 2026
Published: April 13, 2026

Abstract

Early urban planning failed to fully consider the complexities of modern urban underground transportation. For example, underground tunnels passing through viaduct piles and the need for excavation of foundation pits beneath the viaduct piles for underground structure construction all significantly impact the stability of existing bridge systems. This paper studies the stability of viaduct piles after replacement due to deep foundation pit excavation. Based on the preliminary tunnel project of the Nanjing South Road Viaduct, a pile replacement scheme is designed, a three-dimensional numerical model of the viaduct's stress system is established, and the impact of deep foundation pit excavation on the structure of the replaced viaduct and its surrounding environment is analyzed.

Keywords

Pile Foundation Replacement, Deep Foundation Pit Excavation, Viaduct, Numerical Simulation, Deformation Analysis

1. Introduction

In recent years, with the rapid development of urban infrastructure in my country, the development of pile foundation replacement technology has also received significant attention. Many landmark buildings in cities have a long history and are often located in the city center. Most of these buildings have undergone multiple renovations and reconstructions. New subway lines or municipal tunnels need to pass under existing buildings, thus requiring the use of pile foundation replacement [1] [2] methods to reinforce existing pile foundations. Reinforcing existing pile foundations near these landmark buildings will require substantial manpower and

resources and present further challenges to pile foundation replacement technology.

Many scholars at home and abroad have conducted relevant research on pile foundation underpinning technology through theoretical analysis. Jin *et al.* [3] analyzed the reasonable excavation and exposure depth of pile foundation underpinning construction based on theoretical analysis, and discussed the influence law of underpinning on bridge and surrounding ground settlement. They put forward reasonable excavation and exposure depth experience for similar projects in the future to ensure the safety of bridge structure during construction. Xiang *et al.* [4] estimated the possible settlement after the completion of overpass construction based on theoretical calculation of the underpinning construction process. The results showed that the theoretical calculation results were in high agreement with the measured results, which can provide a reference for similar engineering cases. Makarchian and Poulos [5] explored the stress characteristics of pile foundation underpinning under raft foundation system through theoretical research. The results showed that most of the load was transferred to the raft foundation, which is beneficial to the stability of the upper structure of the building.

During the on-site replacement construction, reasonable construction measures need to be taken to ensure the stability of the on-site building structure. Park *et al.* [6] proposed and verified an improved pile foundation replacement support method. The on-site application results showed that compared with the traditional pile driving technology, this method can shorten the construction period by 1.5 times and the construction cost by 1.2 times. When Tokai Railway Company excavated a new subway line under Nagoya Station, it used temporary structures and newly built pile foundations as the load-bearing replacement system to improve the safety of underground construction. This pile foundation replacement method saved a lot of construction time and cost [7]-[9]. Goh *et al.* [10] analyzed the internal force and displacement response characteristics of a complex static uncertain structure composed of bridge superstructure-pile-soil under different jacking loads. Deng *et al.* [11] combined the pile foundation replacement project of a shield tunnel under a three-span simply supported beam bridge in Fuzhou as the research background, and combined with the data of on-site monitoring, compared and analyzed the displacement and internal force response law of complex statically indeterminate structures under different jacking loads. Peng *et al.* [12] investigated the deformation law of the existing subway viaduct during the pile foundation replacement construction process for a deep foundation pit project of a road in Beijing. They used pile foundation replacement technology and combined it with monitoring data to analyze the deformation law of the existing bridge structure and verify the feasibility of the pile foundation support scheme. Su *et al.* [13] introduced the different application scenarios of active replacement and passive replacement in the project based on the shield tunnel of Guangzhou Metro Line 21 crossing the existing viaduct pile foundation. They also elaborated on the applicable conditions and construction process of passive replacement. Zhou *et al.* [14] studied the rationality and feasibility of the passive

replacement construction scheme of a viaduct in Guiyang City. In order to ensure the structural safety of the existing viaduct during the pile foundation replacement construction process, they monitored the settlement of the viaduct piers in real time and conducted a detailed analysis of the bridge deck settlement, existing pile deformation, and surrounding ground surface. The monitoring results showed that after the existing bridge piles were cut off, the load of the upper structure of the bridge could be stably transferred to the supporting load-bearing platform, which proved the rationality and feasibility of the construction scheme. Zhou [15] combined the replacement project of the existing elevated bridge pile foundation before the shield tunnel passes through the existing elevated bridge pile foundation, and discussed the existing pile foundation replacement experience and construction technology. He also made a detailed discussion on the replacement construction technology of the shield tunnel before the elevated bridge pile foundation, which provides an important reference for the construction and design of similar pile foundation replacement. Yue *et al.* [16] replaced the pile foundation of a newly built hospital in a dense building complex in a certain area of Shanghai in order to protect the surrounding historical buildings. Practice shows that the construction of the new hospital after the pile foundation replacement has little impact on the surrounding buildings and the ground surface, and ensures the structural safety of the historical buildings.

Unlike most existing studies that focus either on pile underpinning or deep foundation pit excavation as isolated processes, this study addresses a combined engineering scenario involving pile replacement followed by deep foundation pit excavation beneath an operating urban viaduct. This coupled construction sequence introduces complex soil-structure interaction and unloading effects that have not been sufficiently explored in previous research. Methodologically, a three-dimensional numerical model of the viaduct-pile-soil system is established and validated using full-scale field monitoring data, including retaining structure displacement, ground settlement, and support axial forces. This combined numerical-monitoring approach improves the credibility of the simulation results and provides a robust framework for engineering evaluation. From an engineering perspective, this study elucidates the mechanical response of newly replaced piles under excavation-induced unloading, with particular emphasis on the evolution of axial force redistribution and negative skin friction. The findings are transferable to similar urban bridge-tunnel projects where pile replacement and deep excavation are conducted in close proximity.

This paper, based on the foundation pit project of the municipal tunnel under the Nanjing South Bridge viaduct, introduces the design scheme and construction difficulties of the viaduct pile replacement, and uses numerical simulation to analyze the impact of the replacement construction on the viaduct and its surrounding environment. For the deep foundation pit excavation project under the viaduct after the replacement, a three-dimensional numerical model is established, and the simulation results are compared with measured data to verify the model's rationality. Further analysis is conducted on the impact of changes in the stiffness

of the retaining structure, the dimensions of the internal supports, and the thickness of the abutments on the stability of the viaduct.

2. Design of Replacement Scheme for Elevated Bridge Pile Foundation

2.1. Project Overview

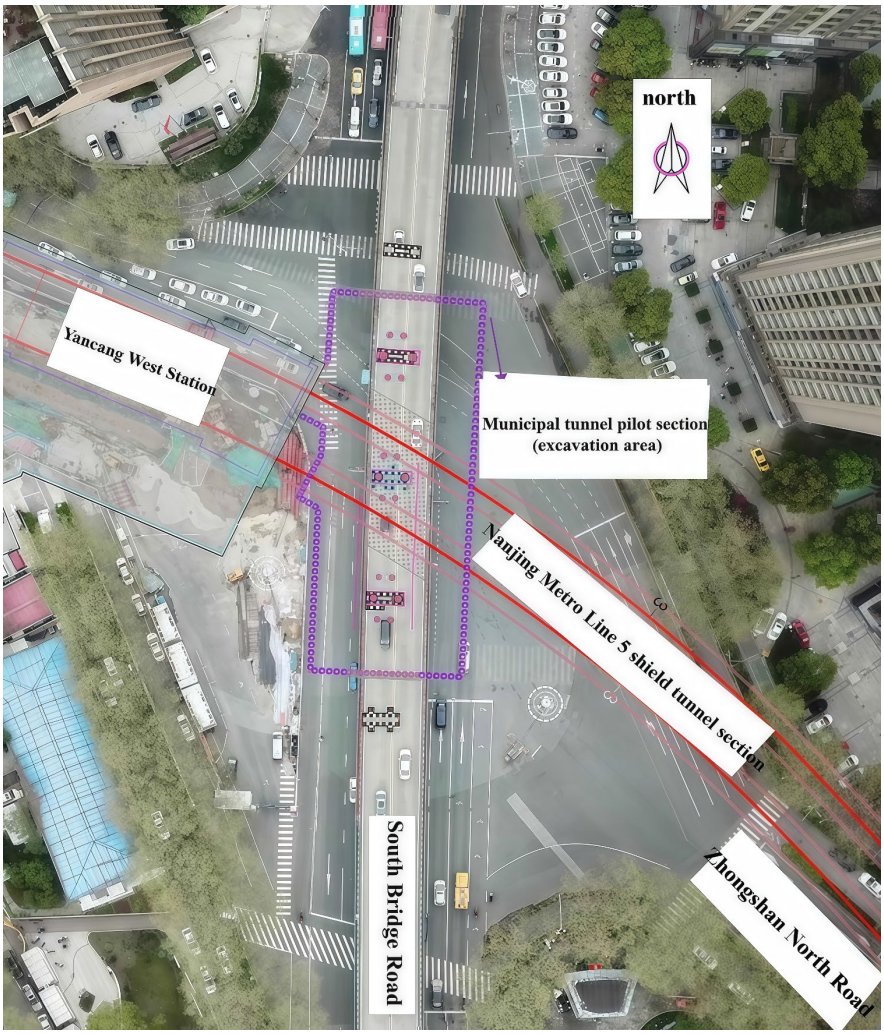

Figure 1. Schematic diagram of the intersection of the first phase of the Daqiao south road municipal tunnel and metro line 5.

This article focuses on the preliminary section of the open-cut tunnel project beneath the Nanjing Bridge South Road Elevated Bridge, located at the intersection of Nanjing Bridge South Road and Zhongshan North Road. As shown in Figure 1, the Nanjing Bridge South Road Elevated Bridge runs north-south, while Zhongshan North Road runs southeast-northwest. Nanjing Metro Line 5 is being constructed along Zhongshan North Road, and this section of the tunnel, using a shield tunnel, crossed the Nanjing Bridge South Road Elevated Bridge in June 2023. The metro station, Yancangqiao Square Station, is located on the northwest

side of the intersection. However, in the long-term plan, the Nanjing Bridge South Road Elevated Bridge will be converted into a municipal tunnel, which will be constructed using a two-way six-lane open-cut method. The under-construction Metro Line 5 tunnel section has approximately 10 m of overburden on the Nanjing Bridge South Road section, with only a 1 m clearance between its bottom slab and the planned Nanjing Bridge South Road municipal tunnel. Due to the requirements for deformation and buoyancy resistance of the metro tunnel section, the planned municipal tunnel cannot be constructed above Metro Line 5. Therefore, it is necessary to first construct a section of the municipal tunnel near the shield tunneling area (referred to as the preliminary section of the municipal tunnel). This preliminary section will be constructed using the open-cut method, with a north-south length of 70.5 m and an east-west length of approximately 27.5 m, reaching a depth of about 10 meters, approaching the ends of the precast piles under the Nanjing South Road viaduct. Therefore, to ensure the safe operation of the existing Nanjing South Road viaduct, it is necessary to reinforce and protect the viaduct's pile foundations before proceeding with the excavation of the preliminary section of the municipal tunnel.

2.2. Engineering Geological and Hydrogeological Conditions

The proposed site for the initial section of the municipal tunnel is located in the floodplain area of the Qinhuai River, where sandy soil and silt are both developed, the groundwater level is high, and the engineering geological conditions are moderate. According to the detailed geotechnical investigation report, the soil layers at the site are divided into 10 categories. The engineering geological characteristics and distribution of each soil layer are detailed in Table 1. Overview of stratigraphic distribution and characteristics within the proposed project area.

Table 1. Overview of stratigraphic distribution and characteristics within the proposed project area.

Stratigraphic age	Stratum number		Stratigraphic name	Distribution range	Burial depth of the layer (m)	Thickness (m)
	Layer	Sub-layer			Minimum - Maximum	Minimum - Maximum
Q_4^3	①	①-1	Miscellaneous fill	Widely distributed	0.60 - 3.90	0.6 - 3.90
		①-2	Plain fill soil	Local missing	1.50 - 3.20	0.70 - 2.80
		①-3	silty fill	Local distribution	2.30 - 4.70	0.70 - 2.60
Q_4^{2-3}	②	②-1d3	silt	Widely distributed	5.60 - 10.70	2.20 - 8.30
		②-2c3	silt	Widely distributed	8.20 - 19.10	1.30 - 2.30
		②-3d1-2	silt	Most of the fabric	19.8 - 20.20	1.10 - 1.50
J	J3	J3l-2	andesite	Local distribution	8.70 - 21.70	0.40 - 1.60
		J3l-3	andesite	Not exposed		
J	J1-2x	J1-2x-2	Muddy sandstone, sandy mudstone	Local distribution	15.80 - 23.00	0.30 - 3.00
		J1-2x-3	Muddy sandstone, sandy mudstone	Not exposed		

The groundwater at the proposed site can be mainly classified into two types: phreatic water and fissure water. The former is located in the upper loose layer, while the latter exists in the bedrock weathering zone. The phreatic water aquifer includes fill, recently deposited silt, and silty sand layers. The silty sand layer ②-1d3, silty soil layer ②-2c3, and silty sand layer ②-3d1-2 at the proposed site have strong permeability. The bedrock weathering fissure water aquifer is mainly composed of Jurassic Xiangshan Group argillaceous sandstone and Jurassic Longwangshan Formation andesite. The fissure water is mainly located at the top of the strongly weathered rock, connected to the upper sand and silt layers. Overall, it has good water-bearing capacity, and the bedrock fissure water level is basically level with the upper phreatic water level.

2.3. Pile Foundation Underpinning Design Scheme

The Nanjing Bridge South Road Elevated Bridge is a main thoroughfare on Huju North Road in Nanjing, leading to the Nanjing Yangtze River Bridge. The bridge foundation uses 40 cm × 40 cm precast reinforced concrete square piles, each 25 m long. The excavation depth of the tunnel pit beneath the elevated bridge is approximately 10 meters. To ensure the safe operation of the existing elevated bridge, the foundations of the elevated bridge sections (50#, 51#, and 52#) located within the pit must be reinforced and protected before the pit construction begins. Figure 2 shows a schematic diagram of the original bridge pile structure; the original abutments were irregularly shaped. Therefore, in the numerical model, the abutments were simplified as equivalent prismatic three-dimensional solid entities with uniform cross-sections. The overall dimensions, elevation, and load-bearing surfaces were preserved, and the contact interfaces between the abutments, piles, and surrounding soil were explicitly maintained. Minor geometric irregularities that have limited influence on global stiffness and load transfer behavior were omitted.

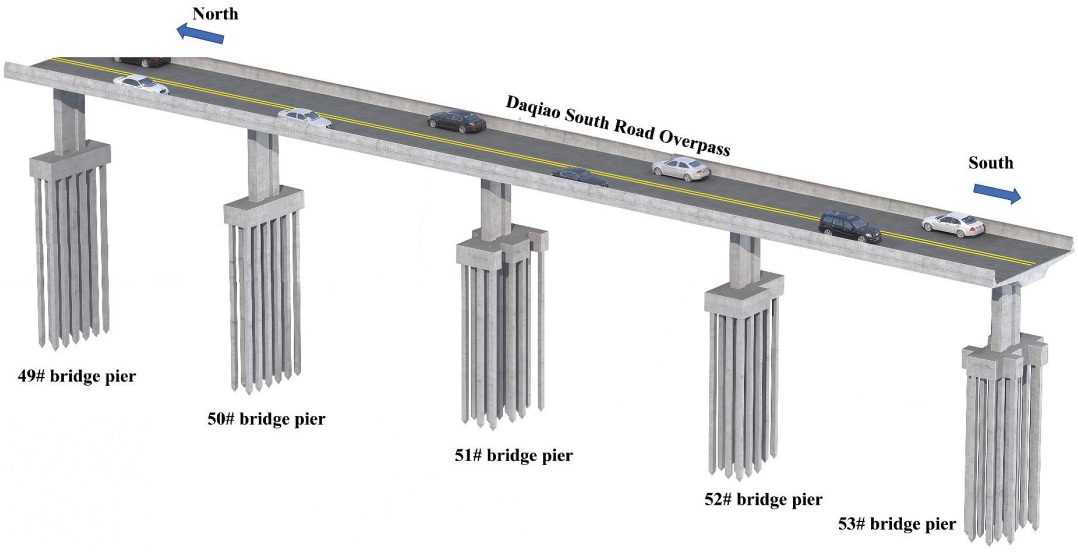

Figure 2. Original bridge pile structure diagram.

The newly constructed piers #50, #51, and #52 are identical in design to the old piers, measuring 3 m in length, 0.9 m in width, and 6.5 m in height. The new abutments are 8 m long, 2.4 m wide, and 2.3 m high. The new bridge pile foundations are double-pile foundations connecting the abutments, with piles 1.5 m in diameter and 30 m in length. The piles are bored cast-in-place piles, with the pile bottoms embedded in moderately weathered rock. The minimum clearance between the piles and the outer edge of the subway structure is no less than 0.75 m, and the minimum clearance between the piles and the central partition wall of the municipal tunnel is no less than 0.5 m. Figure 3 shows a schematic diagram of the bridge pile structure after the replacement.

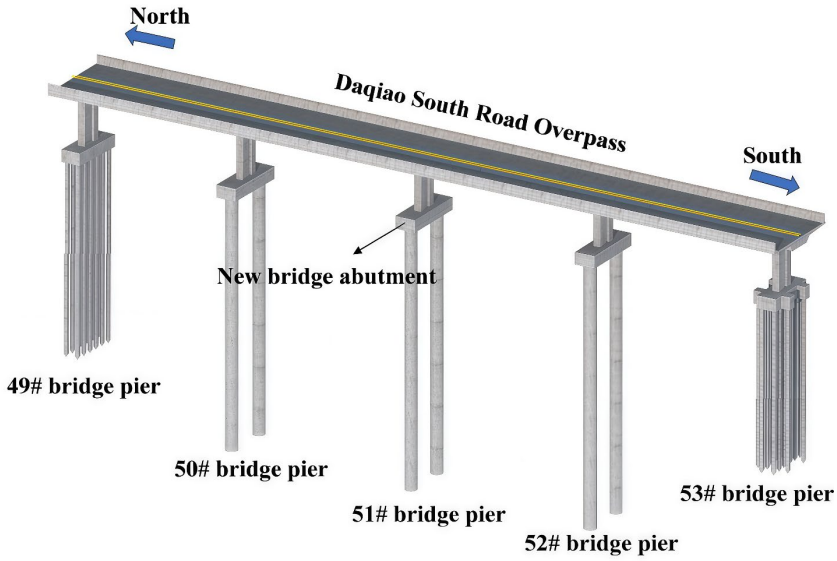

Figure 3. Schematic diagram of the bridge pile structure after replacement.

3. Analysis of the Impact of Deep Foundation Pit Excavation on the Underpass and Surrounding Environment

3.1. Foundation Pit Excavation Model Establishment

To investigate the impact of deep foundation pit excavation directly beneath the viaduct on the viaduct system and its surrounding environment, the entire excavation process was simulated using finite element method software. The excavation depth was 10.3 m, the length was 70 m, and the width was 27.5 m. The tunnel was constructed using the open-cut method. The soil dimensions of the model site were 180 m × 125 m × 45 m, and the three-dimensional finite element model is shown in Figure 4. The positional relationship between the foundation pit and the viaduct pile foundation is shown in Figure 5.

In the numerical model, the soil adopts a modified Mohr-Coulomb constitutive model. The interaction between the pile and surrounding soil was simulated using interface elements. The interface friction angle δ was taken as 0.7 times the soil internal friction angle φ, $\delta = 0.7\varphi$, while the interface cohesion was neglected. The empirical values for the three basic stiffness parameters in the modified Mohr-

Coulomb constitutive model in Midas GTS NX are as follows: secant stiffness in the standard drained triaxial test, tangential stiffness in the main consolidation apparatus loading, and elastic modulus under elastic unloading/reloading. Among these, n = 4 - 6 exhibits good adaptability. Based on the mechanical property indices provided in the geological exploration report and combined with engineering practice experience, the modified Mohr-Coulomb constitutive model parameters for each soil and rock layer are given, as shown in Table 2. The basic physical and mechanical property indices of each soil and rock layer are shown in Table 3. In the model, the reinforced concrete structures such as bridge decks, piers, abutments, and piles, as well as the moderately weathered andesite, all adopt linear elastic constitutive models. The basic physical and mechanical parameters of each structure are shown in Table 4.

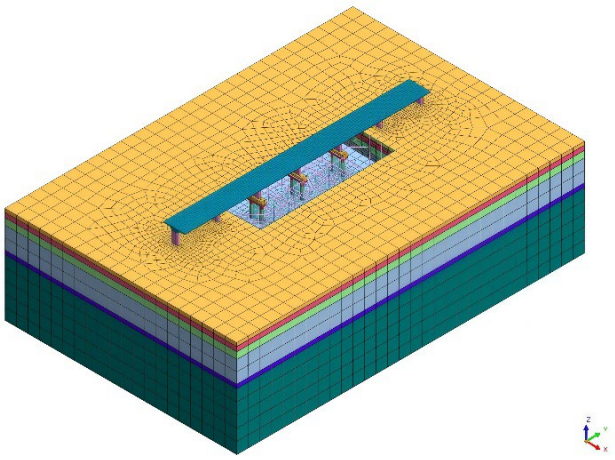

Figure 4. Overall model after foundation pit excavation.

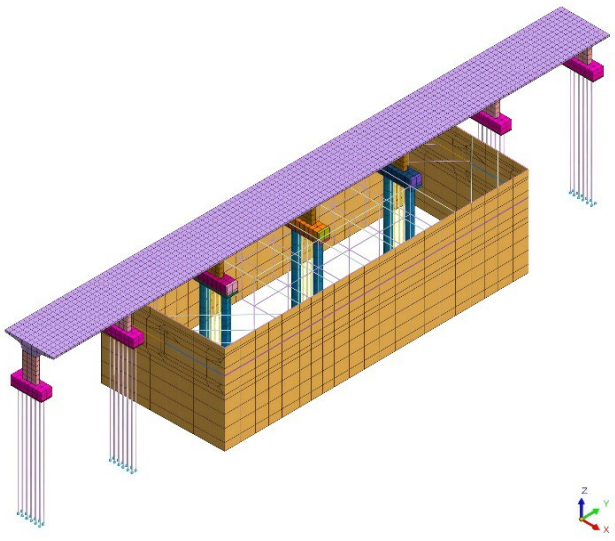

Figure 5. Positional relationship between deep foundation pit and viaduct piers.

The modified Mohr-Coulomb constitutive model was adopted in this study due

to its robustness, limited parameter requirements, and widespread use in engineering practice, which makes it suitable for capturing the overall deformation and internal force response of the bridge-pile-soil system. Soil layers were assumed to be homogeneous, neglecting local spatial variability, in order to represent the dominant mechanical characteristics identified in the site investigation. Temperature effects, construction disturbance, and time-dependent behaviors such as creep and consolidation were not considered, as the analysis focuses on the short-term mechanical response dominated by excavation-induced unloading. A qualitative sensitivity assessment indicates that soil stiffness, pile-soil interface properties, and excavation depth have the greatest influence on ground displacement and pile axial force. Consequently, the model is not intended to capture small-strain stiffness effects or long-term deformation, and the results should be interpreted as reflecting overall mechanical trends rather than precise local responses.

Table 2. Soil basic stiffness parameters.

Soil layer name	E_s/MPa	E_{50}^{ref} /MPa	E_{oed}^{ref} /MPa	E_{ur}^{ref} /MPa
Plain fill soil	4.5	22.5	22.5	67.5
Silty fill	3.17	15.85	15.85	47.55
Silt	9.46	47.3	47.3	141.9
Silt soil	5.53	27.65	27.65	82.95
Strongly weathered andesite	28	140	140	420
Moderately weathered andesite	51	255	255	765

Table 3. Basic physical and mechanical properties of soil and rock in numerical models.

Soil layer name	γ/kN·m^3	Thickness/m	μ	E_s/MPa	c/kPa	φ/˚
Plain fill soil	18.2	1.8	0.38	4.5	10	10
Silty fill	18.1	2.3	0.31	3.17	16.1	12.9
Silt	19.4	3.4	0.28	9.46	8.8	31
Silt soil	17.6	11.1	0.30	5.53	11.1	25.2
Strongly weathered andesite	23.0	2.0	0.23	28	20.8	32.0
Moderately weathered andesite	28.5	29.4	0.15	51	21.3	32

Table 4. Basic physical and mechanical parameters of the structure in the numerical model.

Structural parameters	Unit type	Size/mm	γ/kN·m^3	μ	E/GPa
Old bridge piles	1D Beam unit	400 × 400 × 25000	26	0.2	31.5
New bridge piles	3D Entity unit	1500 × 30000 (Pile diameter × Pile length)	26	0.2	31.5
Bridge piers	3D Entity unit	3000 × 900 × 6500	26	0.2	31.5
Bridge deck	3D Entity unit	11000 × 350 (Width × Thickness)	25	0.25	34.5
Old bridge abutment	3D Entity unit	7000 × 2400 × 2000	26	0.2	31.5
New bridge abutment	3D Entity unit	7000 × 2400 × 2300	26	0.2	31.5

The model's bottom was constrained in both vertical and horizontal directions, while the normal displacement around the model was also constrained. Based on the serviceability limit state calculation results of the superstructure of the Daqiao-nan Road viaduct, the most unfavorable (maximum) value of the pier top support reaction force was applied as a uniformly distributed load to the pier top supports. The uniformly distributed loads on the tops of each pier (48# - 54#) in this model are shown in Table 5.

In the calculation of this model, the traffic load on the bridge deck is taken as 20 kPa, which is applied to the bridge deck, and the gravitational acceleration is 9.8 m/s^2. This value was determined in accordance with the General Specifications for Design of Highway Bridges and Culverts (JTG D60—2015), which recommends an equivalent uniformly distributed traffic load of 20 kPa for urban viaduct decks under normal service conditions. The adopted traffic load represents a standard serviceability load case rather than a specific extreme or worst-case scenario.

Table 5. Uniformly distributed load on bridge piers.

Pier Number	48#	49#	50#	51#	52#	53#	54#
Uniformly distributed load on pier top/kN·m^2	1652.56	1642.42	1900.34	1852.97	1898.29	1896.71	1814.07

Based on the actual working conditions of the bridge south road pile foundation replacement, the analysis steps of the model are set as follows:

1) Establish the initial stress field, activate all soil layers involved in the model, assign the properties of the abutment location to the soil properties of that layer, and clear the initial stress field displacement to zero.

2) Activate the viaduct pile foundation and piers, modify the soil properties of the abutment location to the abutment properties, and apply a uniformly distributed load above the piers.

3) Activate the bridge slab mesh group and apply a uniformly distributed load above the bridge slab, and finally clear the displacement of this construction step to zero.

4) Passivate the structures under bridges 50#, 51#, and 52#, and activate the piers, abutments, and newly built piles of bridges 50#, 51#, and 52#.

3.2. Comparative Analysis of Numerical Simulation Results and Measured Data

To verify the rationality of the finite element numerical model, the field measured data and numerical simulation results were compared and analyzed. Figure 6 shows the layout of the monitoring points for the foundation pit. For deep horizontal displacement, seven sets of observation points (CX1 - CX7) were set up around the perimeter of the foundation pit, with the same depth as the retaining piles. For axial force of the support, seven monitoring points were set up for each layer of support (ZL1 - ZL7 for the first layer of support, ZL8 - ZL14 for the second

layer of support). For surface settlement, seven sets of observation points were set up around the perimeter of the foundation pit, with five surface monitoring points in each set (DB1-1 - DB1-5, DB2-1 - DB2-5, DB3-1 - DB3-5, DB4-1 - DB4-5, DB5-1 - DB5-5, DB6-1 - DB6-5, DB7-1 - DB7-5).

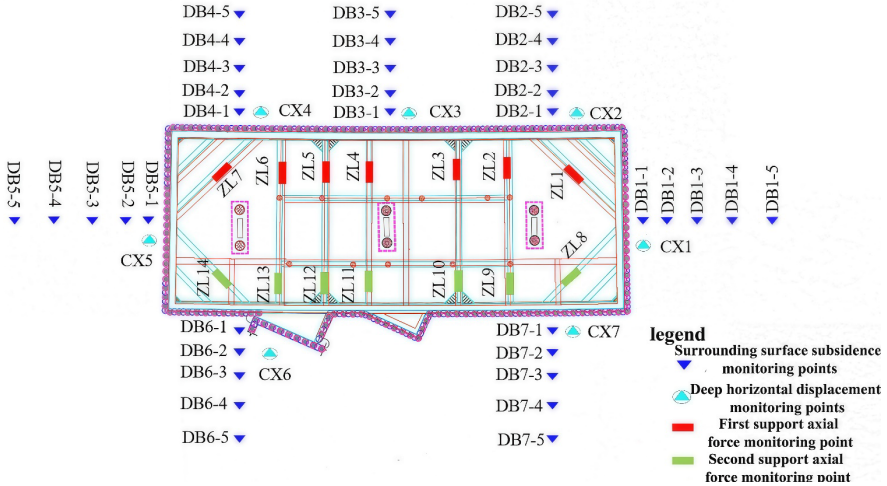

Figure 6. Layout diagram of foundation pit monitoring points.

3.2.1. Horizontal Displacement of Foundation Pit Retaining Structure

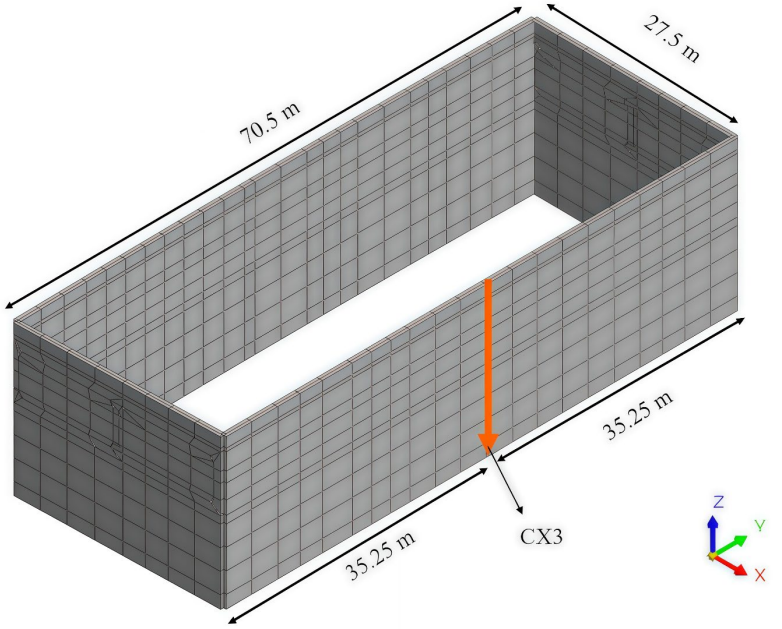

Figure 7. Schematic diagram of the location of survey line CX3.

The horizontal displacement of the retaining structure of an excavation pit can directly reflect the degree of soil disturbance. If the horizontal displacement of the retaining structure is too large, the excavation pit is prone to instability, causing construction safety hazards. Therefore, the horizontal displacement of the retaining structure plays an important role in the stability of the viaduct, surrounding

buildings, and the excavation pit itself. The measured and simulated results of the horizontal displacement of the retaining structure at various points on survey line CX3 under different excavation stages were extracted and compared. The location of survey line CX3 is shown in Figure 7, and the horizontal displacement variation curves at various points on this survey line are shown in Figure 8.

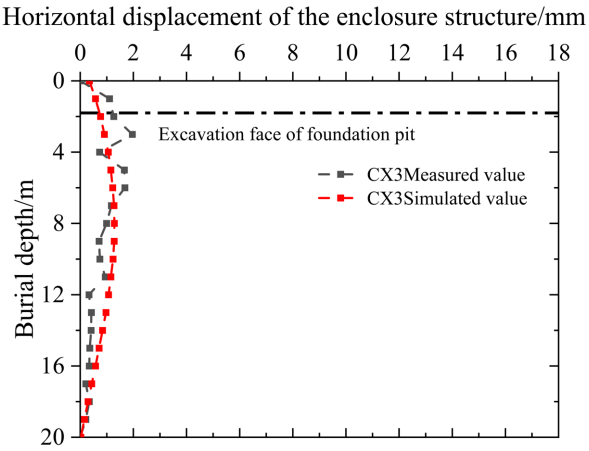

(a) First excavation

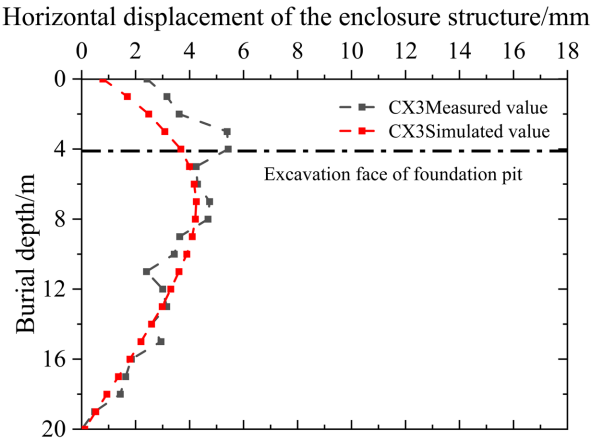

(b) Second excavation

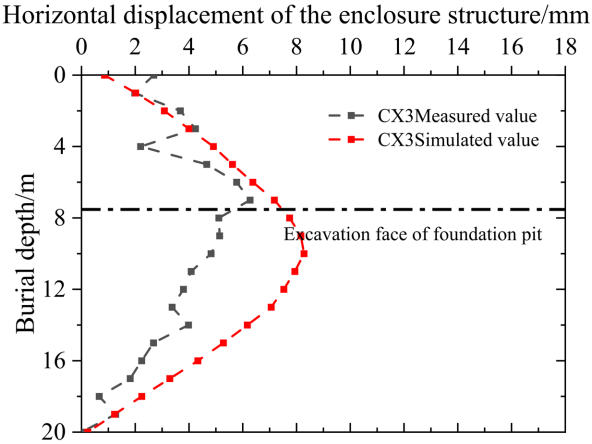

(c) Third excavation

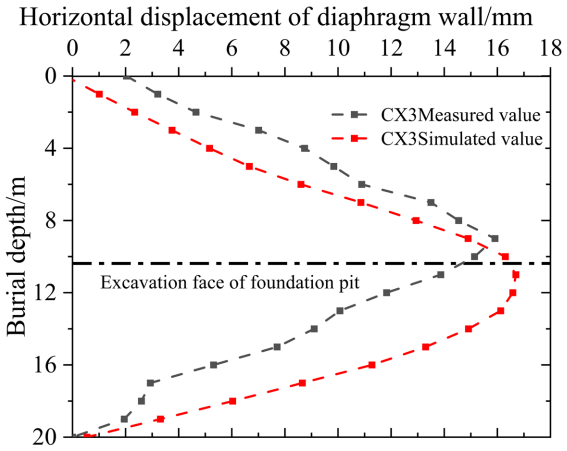

(d) Fourth excavation

Figure 8. Comparison of horizontal displacements of retaining structures at different excavation stages.

As shown in **Figure 8**, the measured and simulated values of the horizontal displacement of the retaining structure exhibit basically the same variation pattern at different excavation stages, verifying the reliability and effectiveness of the numerical model. The maximum horizontal displacement of the retaining structure mainly occurs at the excavation face, with the horizontal displacement values showing a distribution trend of being larger in the middle and smaller at both ends, approaching zero at the bottom of the retaining structure.

Although the overall trend of the numerical results agrees well with the field measurements, certain discrepancies can be observed at specific excavation stages. These differences are not only related to external factors such as construction disturbances and environmental conditions, but are also associated with the inherent limitations of the constitutive model adopted in this study. The Modified Mohr-Coulomb model assumes a constant elastic stiffness and does not explicitly capture the nonlinear stiffness characteristics of soil at small strain levels. In reality, the soil stiffness at small strains is generally higher than that predicted by the MMC model, which may result in an overestimation of deformation during the initial excavation stages. Moreover, time-dependent behaviors such as creep and stress relaxation are not considered in the present numerical model. During prolonged excavation and unloading processes, these effects may contribute to additional deformation accumulation in the field, thereby increasing the divergence between measured and simulated responses.

3.2.2. Surrounding Surface Subsidence

Combining measured and simulated surface settlement values, five measuring points (DB3-1 - DB3-5) of the surface settlement measuring point group DB03 at the pit edge were selected for analysis. The changes in surface settlement with horizontal distance from the pit edge as measured in the field and in numerical simulation are shown in **Figure 9**.

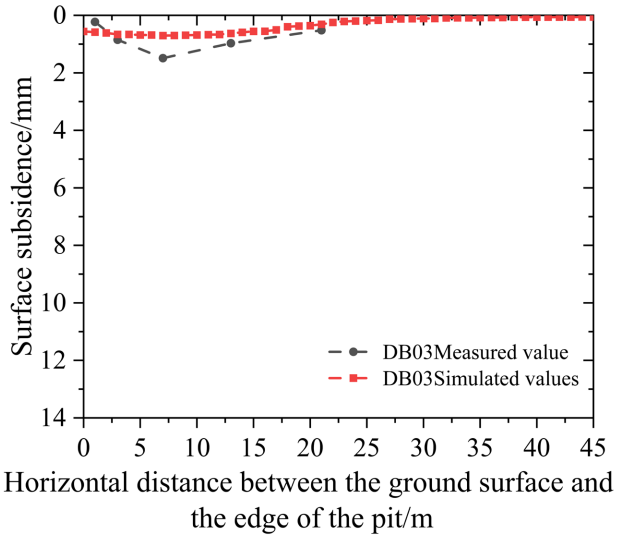

(a) First excavation completed

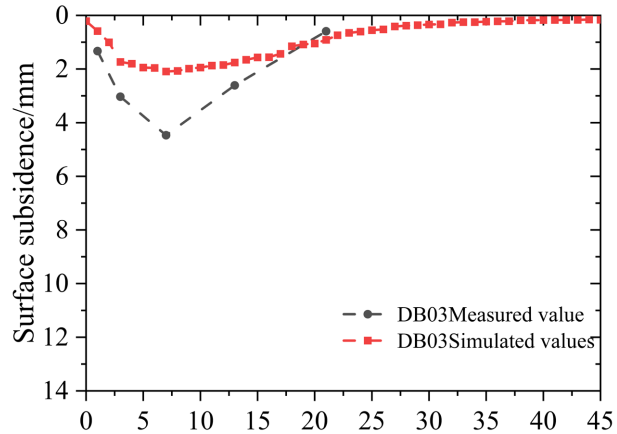

(b) The second excavation has ended

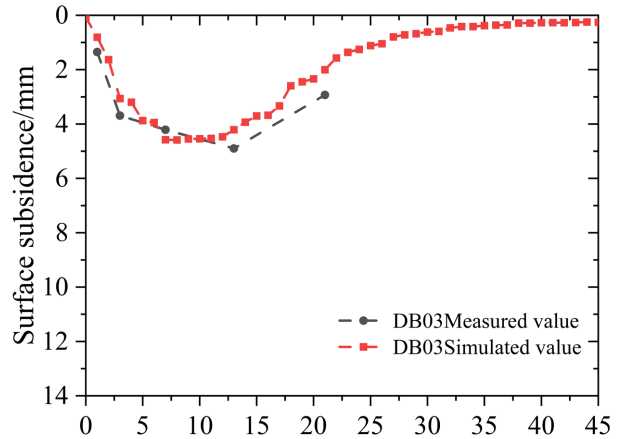

(c) The third excavation has ended

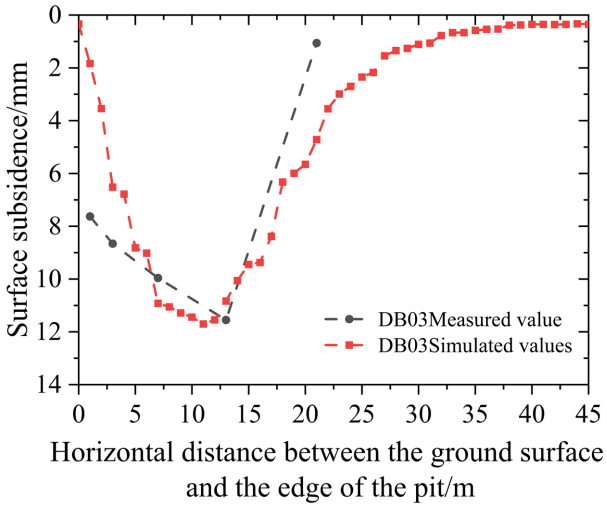

(d) The fourth excavation has ended

Figure 9. Surface settlement curves at different excavation stages.

As shown in **Figure 9**, under different excavation conditions, the measured and simulated values of the surrounding surface settlement generally follow the same trend, exhibiting a "spoon-shaped" distribution along the horizontal distance from the pit edge. However, some differences exist between the two. This phenomenon is caused by two main reasons: Firstly, numerical simulation results are not affected by the external environment. In actual excavation, the increased load on the soil due to the compaction of surrounding heavy machinery leads to increased settlement. Secondly, the soil in the finite element software simulation is uniformly distributed, while the actual soil distribution is uneven, resulting in differences between the measured and simulated results.

As the excavation depth increases, the surface settlement at each measuring point gradually rises, with the impact decreasing the further away from the pit edge. After the excavation is completed, the soil settlement near the retaining structure is not the largest, indicating that the retaining structure provides some support to the pit. The measured settlement value is the largest at 13 m from the pit edge, reaching 11.55 mm. The numerical simulation results show that the surface settlement is greatest at a location approximately 11 m from the edge of the pit, reaching 11.7 mm. Comparison between the measured and simulated results reveals that the calculated settlement results from the numerical model are largely consistent with the measured settlement results, allowing for the prediction of the pit's later deformation patterns.

3.2.3. Support Axial Force

Figure 10 shows a comparison between the measured axial force and the simulation results at each monitoring point. It can be seen that although there is a certain difference between the monitored axial force values and the simulated values, their variation patterns are basically consistent. As excavation progresses, the measured axial force at each monitoring point also increases. For example, at ZL6,

the axial force value at the end of the first excavation is approximately 80 kPa, at the end of the second excavation is approximately 200 kPa, at the end of the third excavation is approximately 550 kPa, and at the end of the fourth excavation is approximately 700 kPa. On-site monitoring is greatly affected by the external environment, causing a sudden change in the axial force value at ZL5 at the end of the second excavation, while the simulated value changes relatively steadily.

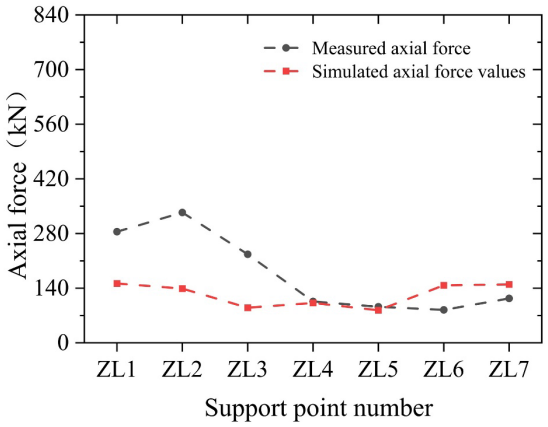

(a) First excavation

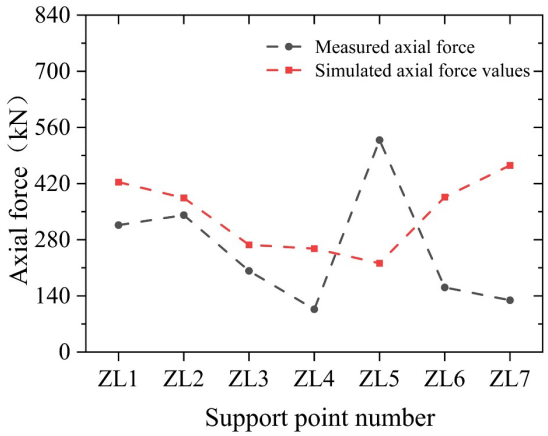

(b) Second excavation

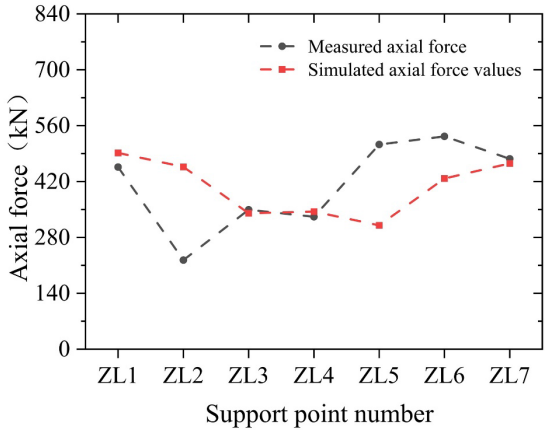

(c) Third excavation

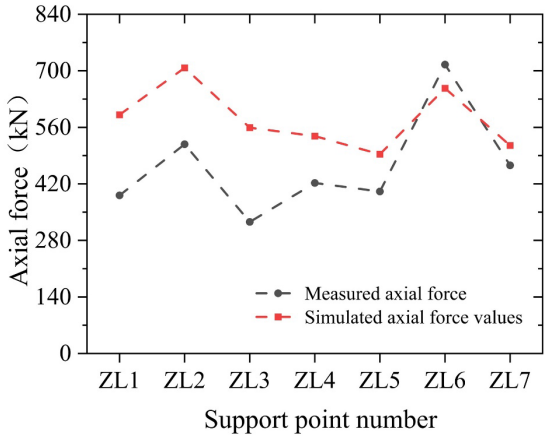

(d) Fourth excavation

Figure 10. Comparison of measured and simulated values of the first support axial force.

3.3. Analysis of the Influence Patterns of Deep Foundation Pit Excavation

This section uses finite element method simulation results to extract and compare numerical values from different measuring points. As the foundation pit is excavated, the horizontal displacement of the retaining structure, the internal forces of the supports, soil settlement, and the internal forces of the viaduct piles are studied to analyze the impact of deep foundation pit excavation on the viaduct piers and bridge decks.

3.3.1. Horizontal Displacement of the Enclosure Structure

During the excavation of the foundation pit, the horizontal displacement of the retaining structure exhibits an "arch-shaped" pattern along the depth direction, with the displacement being larger in the middle and smaller at both ends. **Figure 11** and **Figure 12** show the changes in the horizontal displacement of the retaining structure in the X and Y directions during the excavation process, respectively. It can be seen that as the deep foundation pit excavation progresses, the horizontal displacement of the retaining structure gradually increases. Simultaneously, the location of the maximum displacement gradually shifts downwards along the depth direction of the retaining structure. After excavation, the maximum horizontal displacement of the retaining structure in the X direction is approximately 12 mm, located at a depth of 11 m; the maximum horizontal displacement of the retaining structure in the Y direction is approximately 17 mm, also located at a depth of 11 m. According to the requirements of the "Technical Specification for Monitoring of Building Foundation Pit Engineering" (GB 50497-2019), the warning value for the horizontal displacement of the retaining structure is 18 mm, which does not exceed the warning value specified in the specification. During the foundation pit excavation, it is necessary to monitor the changes in the horizontal displacement of the retaining structure in real time, with particular attention paid to the excavation face.

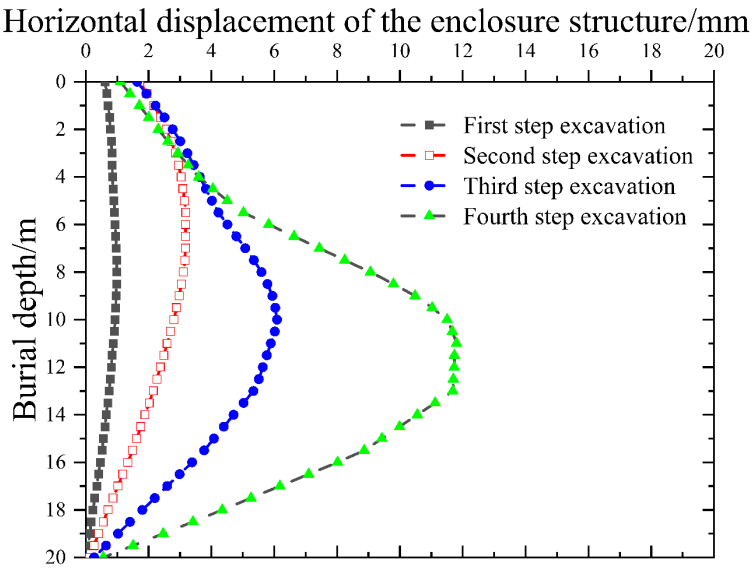

Figure 11. X-direction horizontal displacement curve of the enclosure structure.

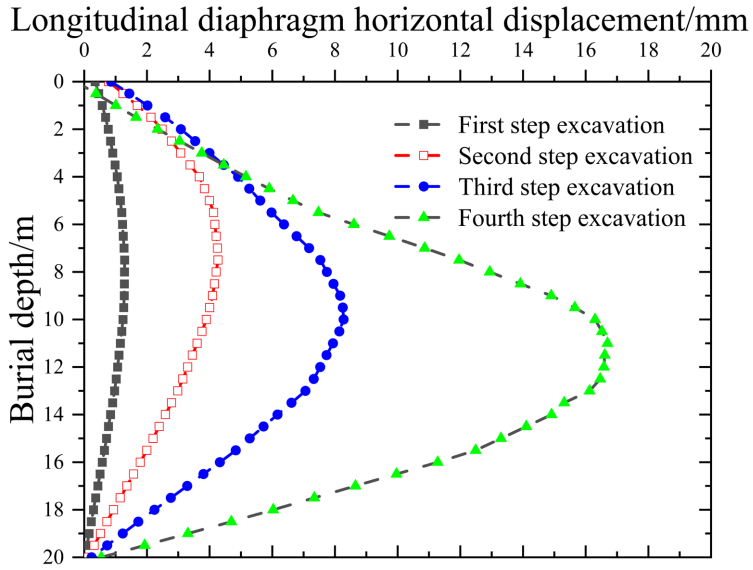

Figure 12. Y-direction enclosure structure horizontal displacement curve.

3.3.2. Surrounding Soil Settlement

As shown in **Figure 13**, the settlement of the surrounding soil layers was relatively small in the initial stage of the excavation. However, the settlement of the ground surface around the pit gradually increased with the increase in excavation depth. At the same excavation depth, the settlement of the ground surface outside the retaining structure in the X direction was greater than that in the Y direction, and both settlement curves exhibited a spoon-shaped distribution. In the X direction, the maximum settlement occurred approximately 11 m from the pit edge, reaching a maximum of 11.7 mm. In the Y direction, the maximum settlement occurred approximately 9 m from the pit edge, reaching a maximum of 3.64 mm.

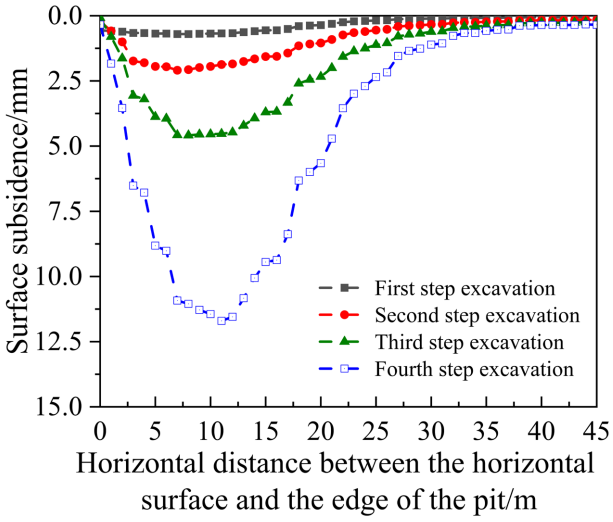

(a) X-direction outer envelope

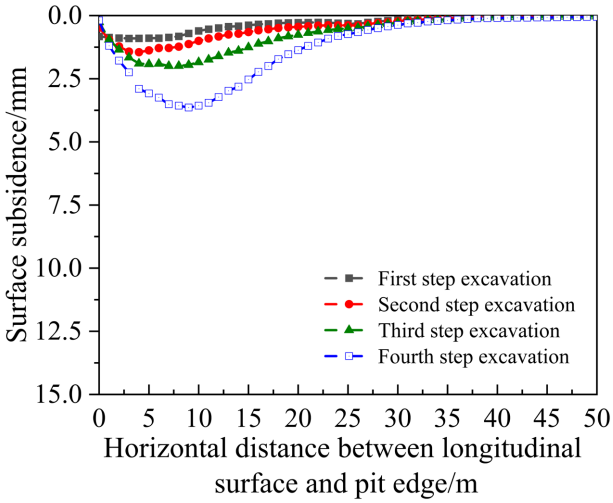

(b) Y-direction enclosure outer side

Figure 13. Surface settlement curve around the foundation pit.

3.3.3. Bridge Deck Deformation

Along the longitudinal direction of the bridge deck, a measuring point was taken every 3.2 meters, resulting in 42 measuring points. The bridge deck settlement variation curve shown in **Figure 14** was plotted. It can be seen that during the excavation of the foundation pit, the bridge deck directly above the pit showed a slight upward convexity. The downward deformation of the bridge deck around the pit increased with the excavation depth, with the largest settlement occurring at the edge of the pit. After the excavation was completed, the maximum settlement of the bridge deck reached 2.369 mm, while the settlement of the bridge deck above the pit was 0.009 mm, resulting in a differential settlement of 2.36 mm, which meets the specifications. During the excavation process, it is crucial to monitor the deformation of the bridge deck above the pit edge to ensure the safe passage of vehicles on the viaduct.

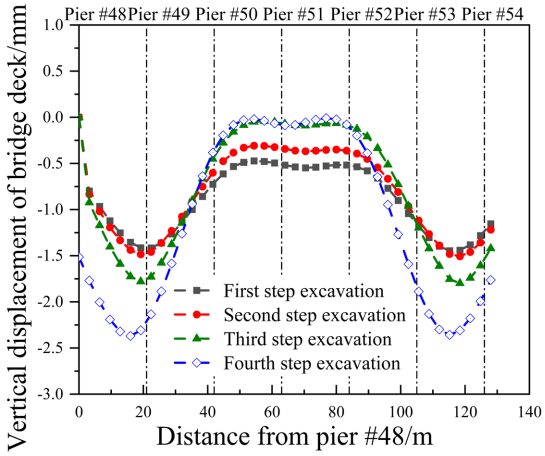

Figure 14. Vertical displacement diagram of bridge deck at each excavation stage.

3.3.4. Supporting Internal Force

Figure 15 shows the axial force cloud diagrams of the supports under different excavation conditions. As can be seen from the figure, due to the large horizontal displacement of the retaining structure at the excavation face, the axial force on the lower supports is relatively large. Therefore, the axial force on the second support is greater than that on the first support. It is worth noting that the second support was installed only after the second excavation was completed; therefore, the axial force values for the second support are only available under the third and fourth excavation conditions.

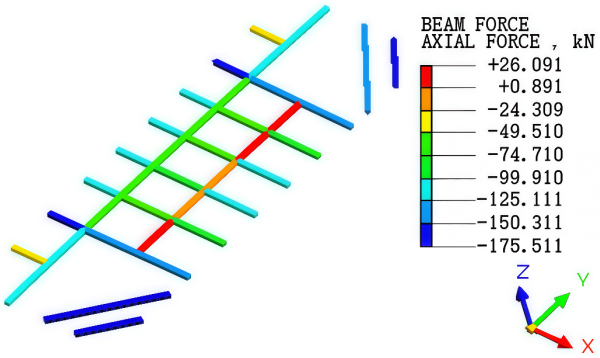

(a) First excavation

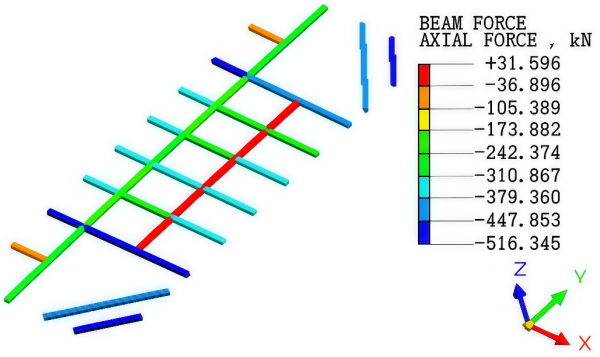

(b) Second excavation

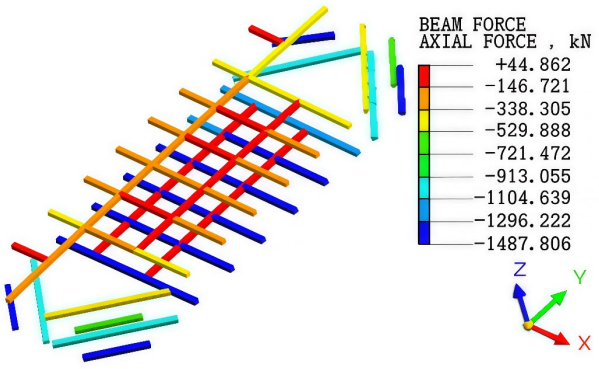

(c) Third excavation

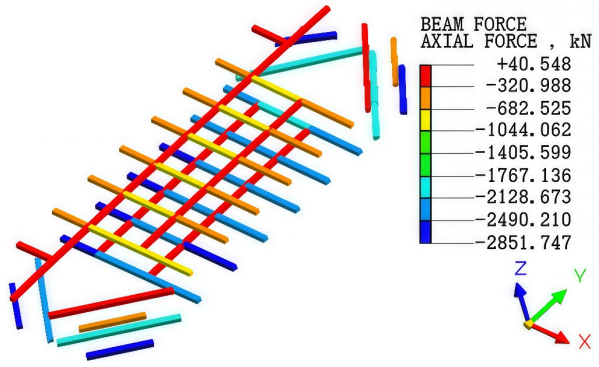

(d) Fourth excavation

Figure 15. Internal support axial force cloud diagram.

3.3.5. Internal Forces of Bridge Piers

Since the bridge pile system at the excavation site is symmetrically distributed and a uniformly distributed load is applied above the bridge, the axial force of half of the bridge pile system, namely piles 48# to 51#, is selected for analysis, as shown in **Figure 16**. The figure shows that pile 48# bears an initial pressure of 200 kN at its top. The axial force decreases with increasing depth, and the axial force at the pile bottom is 31.33 kN, indicating that the skin friction plays a significant role. Because pile 48# is far from the excavated pit, its axial force remains essentially constant with increasing excavation depth. The initial pressure at the top of pile 49# is around 500 kN. The axial force gradually decreases with increasing pile depth, and the axial force at the pile bottom is 53.41 kN. During the excavation process, the axial forces at the pile top and bottom remain relatively constant, while the axial force at the middle of the pile changes significantly. The axial force at the middle of pile #49 reached its maximum value of 608.45 kN after the fourth excavation. The phenomenon of the axial force of pile #49 first increasing and then decreasing is due to the increased horizontal displacement of the foundation pit at the excavation face, which caused the surrounding soil to settle. Under the action of the surrounding soil, the pile generated negative skin friction, which ultimately led to the increase of the axial force at the excavation face.

The newly constructed pile #51 experiences a top pressure of approximately

3800 kN, while the axial force at the pile bottom approaches zero. As the excavation of the foundation pit continues, the axial force on the pile increases. After the third excavation, tensile forces appear on the pile, starting at a depth of 18 m with a value of 68.28 kN. The peak tensile force occurs at a depth of 24 m below the ground surface, reaching 640.44 kN. After the excavation is completed, the peak tensile force shifts downwards, reaching a maximum value of 1287.02 kN at a depth of 26 m. According to the "Code for Design of Concrete Structures" (GB 50010-2010), the design tensile strength of a C30 concrete pile is approximately 1.43 MPa. Therefore, the tensile state of the pile is within the structural safety range.

Inside the foundation pit, the newly constructed 50# bridge pile experiences a pressure of 4000 kN at its top, with the axial force at the pile bottom approaching zero. The axial force decreases with increasing embedment depth. After the third excavation, tensile force appears at a embedment depth of 21 m for 50# bridge pile, with a peak tensile force of 516.20 kN at a depth of 23 m above ground. After the foundation pit excavation is completed, the peak tensile force shifts downwards, reaching a peak of 1141.63 kN at an embedment depth of 26 m.

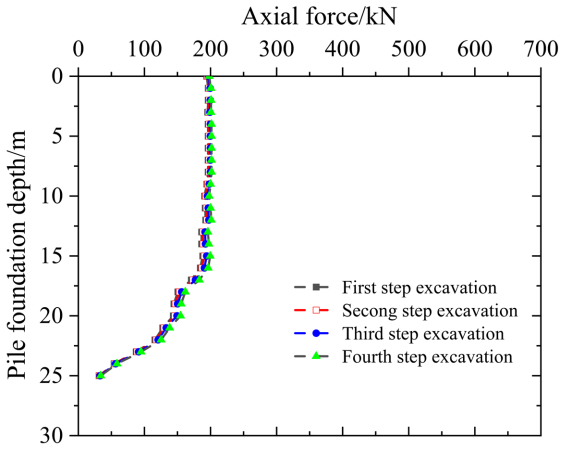

(a) 48# bridge pier

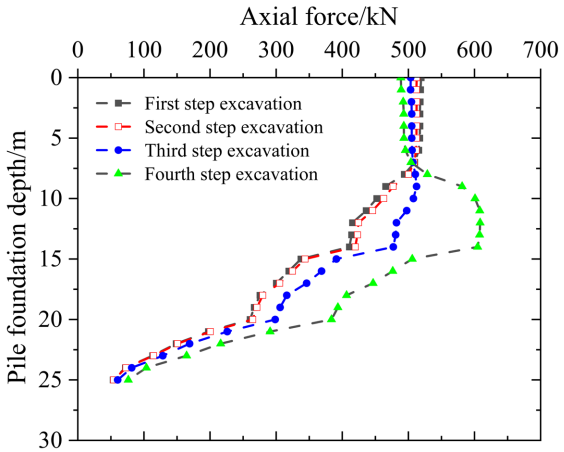

(b) 49# bridge pier

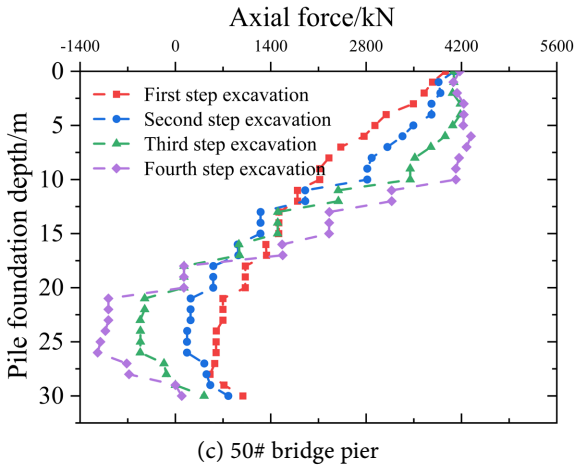

(c) 50# bridge pier

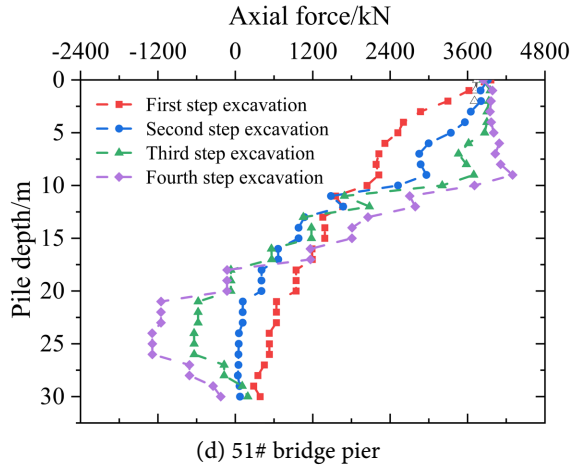

(d) 51# bridge pier

Figure 16. Axial force curves of pile foundations at different excavation stages.

The newly constructed 51# pile experiences a pressure of approximately 3800 kN at its top, with the axial force at its bottom approaching zero. As the foundation pit is continuously excavated, the axial force on the pile increases. After the third excavation of the foundation pit was completed, the pile body experienced tensile force. Tensile force began to appear at a pile depth of 18 m, with a tensile force value of 68.28 kN. The peak tensile force appeared at a position 24 m below the ground surface, with a peak tensile force value of 640.44 kN. After the foundation pit excavation was completed, the peak tensile force shifted downward, with the maximum tensile force value at a position of 26 m, with a peak tensile force value of 1287.02 kN. The simulated pile foundation change trend was basically consistent with the law summarized by Iwasaki *et al.* [17] based on actual measurements.

4. Conclusions

This paper takes the Nanjing Huimin Avenue bridge-to-tunnel project as an example and studies the stability of the elevated bridge pile foundation after pile replacement and deep foundation pit excavation. Based on the current research

status both domestically and internationally, finite element method software is used to simulate the impact of pile replacement and foundation pit excavation on the elevated bridge pile foundation and surrounding soil. Simultaneously, the simulated and measured values of horizontal displacement of the retaining structure, axial force of the supports, and soil settlement at different excavation depths are compared to verify the feasibility of the model, and the following conclusions are drawn:

1) During the excavation of deep foundation pits, the horizontal displacement of the retaining structure gradually increases with the excavation depth, reaching a maximum of 17 mm when the pit is reached. After each excavation stage, the horizontal displacement of the retaining structure along the long side is greater than that along the short side, and the maximum value of the horizontal displacement is mainly concentrated at the excavation face. Therefore, in actual engineering, it is necessary to focus on monitoring the horizontal displacement along the long side of the foundation pit, rationally arrange corresponding monitoring points, and take timely reinforcement measures to control the deformation of the foundation pit when the horizontal displacement of the retaining structure at the excavation face is too large. Increasing the stiffness of the temporary steel support system is shown to be the most effective measure for controlling excavation-induced deformation and limiting the growth of pile axial force. In addition, applying pre-loading to the supports before subsequent excavation stages can reduce initial structural deformation and improve overall system stability. Soil strengthening measures, such as local grouting or ground improvement in the vicinity of the piles and abutments, are particularly effective in mitigating adverse soil-structure interaction effects and reducing deformation concentration.

2) As the deep foundation pit was continuously excavated, the settlement of the surrounding ground surface gradually increased, reaching a maximum of 13.4 mm，exhibiting a spoon-shaped distribution pattern, highlighting the importance of layered excavation for deep foundation pits. Due to the vertical displacement of the soil at the pit's edge, the bridge deck settlement at the pier location near the pit is greater than that at other locations. With increasing distance, the bridge deck settlement gradually decreases. However, the bridge deck inside the pit shows a slight upward trend. This is because the soil inside the pit heaves under unloading conditions during excavation. Furthermore, the reduced bearing capacity of the pile foundations inside the pit due to excavation unloading is also a key consideration in the design.

3) The axial force of the foundation pit supports also exhibits a corresponding variation pattern with the horizontal displacement of the retaining structure. As the foundation pit is continuously excavated, the horizontal displacement of the retaining structure is greatest at the excavation face. Therefore, after excavation, a trend emerges where the axial force of the upper supports is smaller, and the axial force of the lower supports is larger. Comparison of measured and simulated data reveals a high degree of agreement between the horizontal displacement of the

retaining structure, the settlement of the surrounding soil, and the axial force of the supports. This data can effectively predict the impact of deep foundation pit excavation on the elevated bridge directly above and the surrounding environment.

This study provides new insights into the performance of viaduct pile foundations subjected to combined pile replacement and deep foundation pit excavation. By integrating three-dimensional numerical simulation with full-scale field monitoring, the reliability of the predicted deformation and internal force responses is significantly enhanced. The results highlight the importance of excavation-induced unloading effects on newly replaced piles, particularly the development of negative skin friction and tensile forces, which are not adequately addressed in conventional underpinning design approaches. The proposed analysis framework and findings can serve as a reference for similar urban bridge-tunnel projects under complex construction conditions.

Conflicts of Interest

The authors declare no conflicts of interest regarding the publication of this paper.

References

[1] Li, H., Tang, Y., Liao, S. and Shen, M. (2021) Structural Response and Preservation of Historic Buildings Adjacent to Oversized Deep Excavation. *Journal of Performance of Constructed Facilities*, **35**, Article ID: 4021095. https://doi.org/10.1061/(asce)cf.1943-5509.0001676

[2] Liang, F., Cao, P. and Qin, H. (2020) Influence of Excavation beneath Existing Building on Dynamic Impedances of Underpinning Pile Considering Stress History. *Journal of Central South University*, **27**, 1870-1879. https://doi.org/10.1007/s11771-020-4414-y

[3] Jin, F.F., Xu, Q.W., Ma, Z.Z., Ma, J. and Ming, J. (2012) Study on the Pile Exposure Length during the Construction Process of Pile Underpinning under the Road Bridge. *Chinese Journal of Underground Space and Engineering*, **8**, 396-403. (In Chinese)

[4] Xiang, Y., Jiang, Z. and He, H. (2008) Assessment and Control of Metro-Construction Induced Settlement of a Pile-Supported Urban Overpass. *Tunnelling and Underground Space Technology*, **23**, 300-307. https://doi.org/10.1016/j.tust.2007.06.008

[5] Makarchian, M. and Poulos, H.G. (1996) Simplified Method for Design of Underpinning Piles. *Journal of Geotechnical Engineering*, **122**, 745-751. https://doi.org/10.1061/(asce)0733-9410(1996)122:9(745)

[6] Park, Y., Kim, J. and Cho, K. (2015) Stability Analysis of Subway Box Structure Supported by Modified Underpinning Method. *Tunnelling and Underground Space Technology*, **50**, 199-208. https://doi.org/10.1016/j.tust.2015.06.013

[7] Masuda, Y., Minoshima, T. and Makino, H. (1992) Large-scale Underpinning for an Underground Urban Railway Station. *Tunnelling and Underground Space Technology*, **7**, 133-140. https://doi.org/10.1016/0886-7798(92)90043-h

[8] Vynnykov, Y.L., Kharchenko, M.O. and Manzhalii, S.M. (2021) Reinforcement of a Deformed Structure on the Pile Foundation. *IOP Conference Series: Materials Science and Engineering*, **1021**, Article ID: 012030. https://doi.org/10.1088/1757-899x/1021/1/012030

[9] Shan, H., He, S., Lu, Y. and Jiang, W. (2020) Case Study and Numerical Simulation of Excavation beneath Existing Buildings. *Advances in Civil Engineering*, **2020**, Article ID: 8817339. https://doi.org/10.1155/2020/8817339

[10] Goh, A.T.C., Zhang, W., Zhang, Y., Xiao, Y. and Xiang, Y. (2018) Determination of Earth Pressure Balance Tunnel-Related Maximum Surface Settlement: A Multivariate Adaptive Regression Splines Approach. *Bulletin of Engineering Geology and the Environment*, **77**, 489-500. https://doi.org/10.1007/s10064-016-0937-8

[11] Deng, T., Guan, Z.C., Chen, K.L. and Liu, Y. (2015) Simplified Calculation of Jacking Load in Active Underpinning of Bridge Piles. *Rock and Soil Mechanics*, **36**, 3259-3267. (In Chinese)

[12] Peng, H., Peng, X., Wang, G., Li, H., Ma, W., Xiao, X., *et al.* (2021) Research on Deformation Laws of Existing Subway Viaducts Undertravesed by Deep Road Foundation Pit Using Pile Underpinning Technology. *Fifth International Conference on Traffic Engineering and Transportation System* (*ICTETS* 2021), Chongqing, 24-26 September 2021, 727-734. https://doi.org/10.1117/12.2619728

[13] Su, M. and Yin, Z.Q. (2020) Construction Technology of Pile Foundation Exchange and Cutting for Shield Tunneling under Viaduct Piles. *Urban Mass Transit*, **23**, 175-179. (In Chinese)

[14] Zhou, Y., Liu, Y., Chen, Q., Ou, X. and Li, Y. (2022) Case Study of an Underpinning Pile Foundation for an Interval Tunnel Crossing an Existing Bridge. *Applied Sciences*, **12**, Article 12566. https://doi.org/10.3390/app122412566

[15] Zhou, S.J. (2017) Underpinning Scheme Design of Pile Foundation Crossing through the Flyover Bridge. *Chinese Journal of Underground Space and Engineering*, **13**, 162-169. (In Chinese)

[16] Yue, J.Y., Yao, J. and Huang, S.M. (2011) Design and Practice of Deep Foundation Pit Engineering under Sensitive Conditions in Soft Soil Area. *Chinese Journal of Geotechnical Engineering*, **33**, 278-284. (In Chinese)

[17] Iwasaki, Y., Watanabe, H., Fukuda, M., Hirata, A. and Hori, Y. (1994) Construction Control for Underpinning Piles and Their Behaviour. *Géotechnique*, **44**, 681-689. https://doi.org/10.1680/geot.1994.44.4.681